Triplex-Directed Recognition of a DNA Nanostructure Assembled by Crossover Strand Exchange

David A. Rusling,[†,§,*] Iris S. Nandhakumar,[‡,§] Tom Brown,[‡] and Keith R. Fox[†,§,*]

[†]Centre for Biological Sciences, [‡]School of Chemistry, and [§]Institute for Life Sciences, University of Southampton, Highfield, Southampton SO17 1BJ, U.K.

ABSTRACT

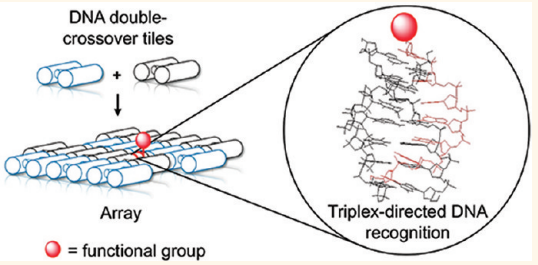

DNA has been widely exploited for the self-assembly of nanosized objects and arrays that offer the potential to act as scaffolds for the spatial positioning of molecular components with nanometer precision. Methods that allow the targeting of components to specific locations within these structures are therefore highly sought after. Here we report that the triplex approach to DNA recognition, which relies on the specific binding of an oligonucleotide within the major groove of double-helical DNA, can be exploited to recognize specific loci within a DNA double-crossover tile and array, a nanostructure assembled by crossover strand exchange. The oligonucleotide can be targeted to both crossover and non-crossover strands and, surprisingly, across the region spanning the crossover junction itself. Moreover, by attaching biotin to the end of the oligonucleotide, we show that streptavidin molecules can be recruited to precise locations within a DX array, with an average spacing of 31.9 (±1.3) nm. This is a promising approach that could be exploited to introduce other components compatible with oligonucleotide synthesis into the wide variety of DNA nanostructures assembled by crossover strand exchange, such as those generated by DNA origami.

KEYWORDS: DNA self-assembly · double-crossover molecule · DX tile · Holliday junction · molecular recognition · triple helix formation

DNA is a very useful material for the self-assembly of objects and arrays with nanoscale dimensions.[1−4] By exploiting Watson−Crick base pairing rules, oligonucleotides can be programmed to assemble in a predefined fashion into complex structures. The design of these structures often relies on the reciprocal exchange of strands between adjacent helices, generating crossovers that act to weave them into two- and three-dimensional layers. This concept was first successfully employed using double-crossover (DX) molecules (or tiles) containing two crossovers connecting collinear duplexes.[5] These tiles have been used to assemble lattices with extensions of several hundreds of nanometers by the inclusion of complementary single-stranded overhangs (sticky ends) at their duplex termini (Figure 1A).[6] This approach has since been extended using double−double-crossover molecules,[7] triple-crossover molecules,[8] and by using multiple crossovers to fold long single-stranded DNA.[9] An alternative strategy that employs strand exchange between helices arranged so they are no longer collinear has also proved successful.[10−14] Both periodic and aperiodic assemblies have been generated in this manner, with a diverse range of applications, including structure determination,[15−17] imaging,[18,19] biosensing,[20,21] electronics,[22] computation,[23−25] and as substrates for chemical and enzymatic reactions.[26,27]

Most of the proposed applications of DNA nanostructures rely on the incorporation of guest molecules into these structures, exploiting the DNA as a "scaffold" or "template" to dictate their spatial positioning. Indeed, a diverse range of molecules, including proteins,[6,10,18−21,28−32] nucleic acid enzymes,[21,33−35] nanoparticles,[6,36,37] and chemical groups,[38] have been incorporated into nucleic acid nanostructures. In each case, the component is chemically attached to one of the template oligonucleotides and added prior to structure assembly or, where applicable, recruited to a group incorporated in the same manner. A limitation of this approach is that a slow annealing step is often required for correct nanostructure assembly, and some components may not tolerate these conditions; proteins for example are denatured at the relatively high temperatures required for annealing. Unwanted side interactions between the component and the assembly might also influence the yield and/or purity

* Address correspondence to d.a.rusling@soton.ac.uk, k.r.fox@soton.ac.uk.

Received for review February 17, 2012 and accepted March 24, 2012.

Published online March 24, 2012
10.1021/nn300718z

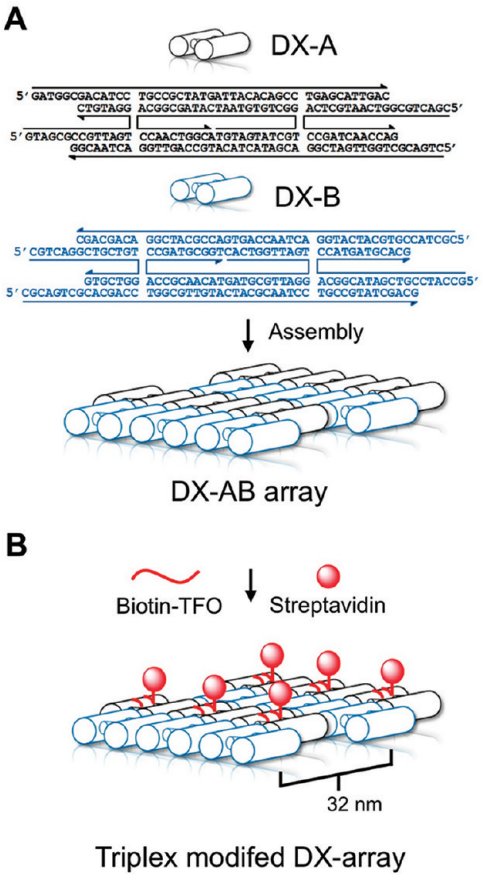

Figure 1. DX tiles and arrays. (A) DX-A tile (black) and DX-B tile (blue) are programmed to contain complementary sticky ends at each of their four duplex termini. The two tiles can be mixed in equal amounts to generate an alternating DX-AB-type array. The sequences of the two tiles are included with the arrows denoting the polarity of the oligonucleotides. (B) Subsequent DNA recognition of a DX-A tile by a TFO conjugated to biotin would allow the protein streptavidin to be recruited to every other tile in the assembly, with a repeat spacing of 32 nm.

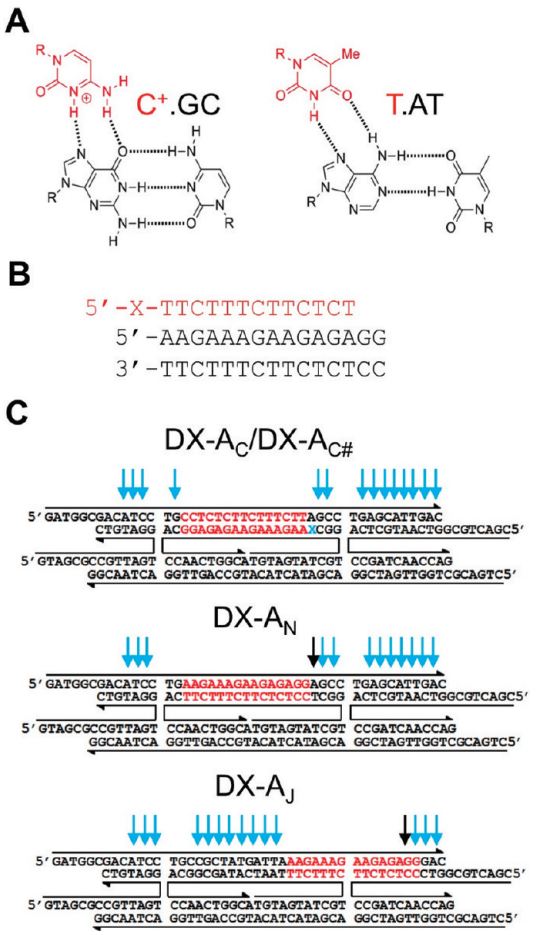

Figure 2. Recognition of a DNA nanostructure by triplex formation. (A) Binding of the TFO generates base triplets, with protonated cytosine recognizing a GC base pair and thymine recognizing an AT base pair. R represents the deoxyribose phosphate backbone. Third strand bases are shown in red and the duplex base pairs in black. (B) Triplex used in this study. The 15 bp oligopurine–oligopyrimidine sequence embedded within the DX-A tile is shown in black and the TFO in red. The TFO was unmodified or had biotin or the fluorescence quencher dabcyl, conjugated at its 5′-end (at position X). (C) Sequences of the modified DX-A tiles used in this study. In each case, the sequence shown in (B) was embedded within the DX tile (shown in red). Two variants of the DX-A_C tile were generated containing either T or FAM-C6-dT at position X within the tile (shown in blue). The latter is referred to as DX-$A_{C\#}$. For each DX tile, the arrows represent regions of the top strand that are susceptible to DNase I cleavage in the presence of TFO and were determined from the cleavage patterns shown in gels in Figure 4B–D). Blue arrows represent cleavage, while black arrows represent regions of enhanced DNase I cleavage at the triplex–duplex junctions.

of the final complex. An alternative approach would be to target the component to a specific double-stranded region within a preassembled structure by conjugating it to a DNA recognition agent (Figure 1B). This has so far proved successful using DNA-binding polyamides.[39] This is a useful advance, but it relies on the compatibility of a particular component with polyamide synthesis.

An alternative strategy is to exploit the triplex approach to DNA recognition, which relies on the specific binding of an oligonucleotide within the major groove of double-helical DNA.[40–43] Triplex-forming oligonucleotides (TFOs) bind in a sequence-specific manner by generating base triplets; TFOs composed of pyrimidine bases bind in a parallel orientation to the central strand of the target duplex, generating C^+.GC and T.AT base triplets (Figure 2A). [The notation X.YZ refers to a triplet in which the third-strand base X interacts with the duplex base pair (bp) YZ, forming Hoogsteen hydrogen bonds to base Y.] Using this recognition code, it is possible to design a TFO to recognize any oligopurine–oligopyrimidine target site, which can be incorporated into a DNA nanostructure by appropriate sequence design. For example, the sequences in Figure 2B show a TFO (in red) designed to recognize a 13 bp region within a 15 bp duplex (in black), positioning a functional group (X) at the 5′-end of the sequence. Unlike other methods of DNA recognition, triplex formation has the advantage that the

TFO is compatible with a variety of modifications that can be conjugated using standard methods of oligonucleotide synthesis. Triplex formation has so far been exploited to recognize a DNA structure containing adjacent hexagonal units constructed using three-way oligonucelotides.[44] Since these structures are not assembled using crossover strand exchange, it has yet to be established whether a TFO has access to this structural motif.

Here we examined the ability of a TFO to recognize and incorporate functionality into a DNA nanostructure assembled by crossover strand exchange, a double-crossover (DX) tile and array. The DX tile (DX-A) is composed of five oligonucleotides, with an antiparallel arrangement of non-crossover strands, and an even number of half-helical turns between crossovers (21 bp). It therefore belongs to the DAE class of DX molecules.[5] The DX array is generated using a second DX tile (DX-B) containing complementary sticky ends at each of the four duplex termini, generating a DX-AB array (Figure 1A). We have used DX sequences that are similar to those used in the original DX study,[6] but since these lacked any oligopurine–oligopyrimidine sites, the sequence shown in Figure 2B was embedded within the DX-A tile (but not the DX-B tile). We chose the DX motif as test system since it allowed us to examine the interaction of a TFO with single DX tiles as well as with DX tiles in the context of a fully formed DX-AB array. The formation of both complexes was characterized by biophysical methods and with the DX-AB array by atomic force microscopy (AFM). Visualization of the bound TFO was achieved by conjugating biotin to the 5′-end of the TFO, which allowed streptavidin molecules to be recruited to precise locations within the nanostructure (Figure 1B).

RESULTS AND DISCUSSION

Targeting of an Isolated DX Tile. Several DX tiles were designed so that they included the 15 bp oligopurine–oligopyrimidine sequence shown in Figure 2B. Initially, this was introduced at a central region between crossovers, leaving at least 2 base pairs between each end of the target sequence and the proximal crossover (Figure 2C). The sequence was introduced in two orientations, with the oligopurine strand located on either the crossover strand or the non-crossover strand, generating DX-A_C and DX-A_N tiles, respectively (Figure 2C). [The notation DX-A_X is used here to refer to each modified DX-A tile, where X refers to location of the purine strand on the crossover (C) or non-crossover (N) strands; the full sequences of all oligonucleotides are shown in Supplementary Table 1 in Supporting Information.] Formation of a triplex on either the DX-A_C or DX-A_N tile positions the central portion of the TFO facing either toward or away from the adjacent helix, respectively.

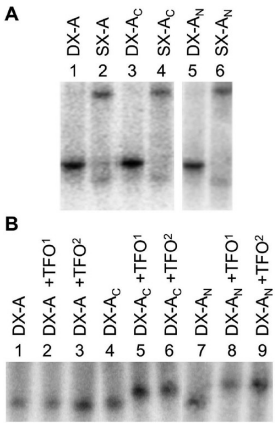

Figure 3. EMSA of DX tiles. The oligonucleotides that made up each DX tile were labeled at their 5′-ends with ^{32}P. These were first annealed at a final concentration of 1 μM before addition of the unlabeled TFO at a final concentration of 10 μM. The complexes were then left to equilibrate for >8 h at 4 °C. Samples were run on a nondenaturing 8% PAGE gel in TA-Mg buffer at 4 °C, and the gel was fixed, dried, and subjected to phosphorimaging. (A) Comparison between complexes containing double-crossovers (DX) and single-crossovers (SX) to ascertain correct structure assembly. (B) Comparison between DX tiles with and without TFO added before[1] or after[2] complex assembly.

Since the original DX-A tile was carefully designed to minimize any sequence symmetry and promote only intended Watson–Crick base pairing, the introduction of the oligopurine sites might influence the formation of the intended structures. The formation of the two new DX-A_C and DX-A_N tiles was therefore compared to the formation of the original DX-A tile using an electrophoretic mobility shift assay (EMSA). All five strands of each tile were labeled with ^{32}P, mixed in stoichiometric amounts, and slowly annealed. The complexes were then subjected to nondenaturing polyacrylamide gel electrophoresis (PAGE). All three complexes generated a single band that ran with the same mobility (Figure 3A; lanes 1, 3, and 5), and about 90% of the strands are incorporated into each tile. The majority of the remaining 10% was traced to the shortest crossover strand, presumably due to its lower affinity for the complex (data not shown). To confirm this, the same experiment was undertaken, but this time, the shortest crossover strand was omitted from the annealing step, generating complexes that contained a single-crossover (SX-A, SX-A_C, and SX-A_N). This time, at least two bands can be seen for each tile with a different mobility to those seen for the full DX tiles (Figure 3A; lanes 2, 4, and 6). The greater flexibility of the two helices in the absence of the second crossover is likely to account for their difference in mobility. These results confirm that these oligonucleotides generate only their intended DX complexes.

To examine whether a TFO was capable of interacting with the tiles, the 13-mer TFO shown in Figure 2B was designed to recognize the 13 base region at the 5′-end of the embedded oligopurine tract. Experiments

were undertaken at pH 5.0 since the formation of a triplex with pyrimidine-containing TFOs requires slightly acid conditions (pH <6.0). An excess of the TFO was added to each tile either before the annealing step or after the formation of the DX tiles. In this way, the accessibility of the TFO to its target site could be compared. The gel in Figure 3B shows that in the absence of TFO all three DX molecules ran with the same mobility (lanes 1, 4, and 7), but in the presence of TFO, a band with a slower mobility is observed for the DX-A_C and DX-A_N tiles (lanes 5 and 8) but not for the DX-A tile that lacks the target site (lane 2). This suggests that the TFO is capable of interacting specifically with its target site irrespective of the strand to which it is targeted. Moreover, the order of TFO addition had no influence on the ability of the TFO to bind, and addition of the TFO after complex formation did not hinder its ability to wrap around its target helix, despite the close proximity of the adjacent helix (lanes 6 and 9). The experiment was repeated with various concentrations of TFO, and the binding was found to be concentration-dependent, as expected for a bimolecular interaction (Supplementary Figure 1).

Although it is clear that the TFO is interacting with each of the DX tiles, the band shift experiments give little information on the structure of the complex formed. Does the TFO cover the entire oligopurine tract? Does binding influence the underlying structure of the DX molecule? To answer these questions, we carried out a DNase I protection assay on the DX tiles in the presence and absence of TFO. DNase I is a double-strand specific endonuclease that generates single strand nicks in the phosphodiester backbone by cleaving the O3′—P bond. Incubation of the enzyme with each of the complexes containing a single ^{32}P-labeled strand (the non-crossover strand) generated labeled fragments that once digested could be separated by denaturing PAGE. Cleavage in the presence of TFO resulted in missing bands or a "footprint" on account of the TFO occluding the action of the enzyme at these positions. This technique therefore revealed regions that had undergone triplex formation. For each complex, a double-stranded (DS-A, DS-A_C, or DS-A_N) equivalent, containing the radiolabeled non-crossover and complementary central crossover strand, was digested for comparison.

The cleavage patterns for the three DX tiles in the presence and absence of various concentrations of the 13-mer TFO are shown in Figure 4. Analysis of the cleavage patterns for the DS and DX complexes in the absence of TFO reveals marked differences (lanes 1 and 3 in each gel). In each case, the regions encompassing the crossover points in the fully formed DX structures (highlighted in bold in the adjacent sequence) are cut poorly relative to the same regions of the DS duplexes. The crossovers clearly occlude the binding and subsequent cleavage by the enzyme. In contrast, there is no difference in cleavage efficiency at the region midway between crossovers, and the enzyme can access these regions equally well. Further analysis of the cleavage patterns reveals extra bands at the 3′- and 5′-ends of the sequences, suggesting that all of the oligonucleotides are bound to their intended partners. Taken together, these results again confirm successful formation of the DX tiles.

Comparison between the lanes in the absence of TFO and those where various concentrations of TFO have been incubated with each DS and DX complex shows clear footprints (underlined region) for the complexes containing an oligopurine target site (Figure 4B,C; lanes 2, 4—6) but not those that lack a target site (Figure 4A; lanes 2, 4—9). The positions of DNase I cleavage in the presence of TFO are shown for each DX tile in Figure 2C (blue arrows). As expected, this is the same for both the DS and DX structures. The binding of the TFO to both DX-A_C and DX-A_N was concentration-dependent, and at lower concentrations, the missing bands reappear. In each case, the size of the binding site is slightly overestimated due to the large size of the enzyme, but the cleavage pattern remains unaltered for the rest of complex, indicating only specific binding of the TFO. A characteristic of DNase I footprints generated by TFOs is hypersensitivity at the triplex—duplex duplex junction, most often observed at the 3′-end of the oligopurine target strand.[45] This is observed for the binding of the TFO to the DX-A_N tile (Figure 2C, black arrows, and Figure 4C, marked by an asterisk) but not the DX-A_C tile (Figure 4B) since this is labeled on the pyrimidine-containing strand.

To confirm that the entire oligopurine sequence is required for binding and that the TFO is not simply tethered to one end of the site, a further DX tile containing only half of this sequence (DX-A_H) was designed. The tile was again based on the DX-A tile, but this time, only the first 6 bp of the oligopurine—oligopyrimidine site shown in Figure 2B was embedded into the complex. Digestion of the complex in the presence of the TFO revealed no change in cleavage pattern, even at a 300-fold higher concentration (Supplementary Figure 2). The interaction of the TFO with its full oligopurine target site is therefore required for the interaction of the TFO with the DX tile.

We next examined whether longer TFOs could interact with a DX tile in the same manner. The incorporation of the 15 bp oligopurine—oligopyrimidine target site into DX-A_N generated a 17 base oligopurine tract and allowed two further TFOs to be designed: a 15-mer and 17-mer containing two or four further nucleotides at their 5′-ends (TFO2 and TFO3, respectively; Supplementary Table 1). The interaction of these two oligonucleotides with the DX-A_N tile was examined by DNase I cleavage, and the digestion patterns for these complexes are shown in Supplementary Figure 3A,B. Again,

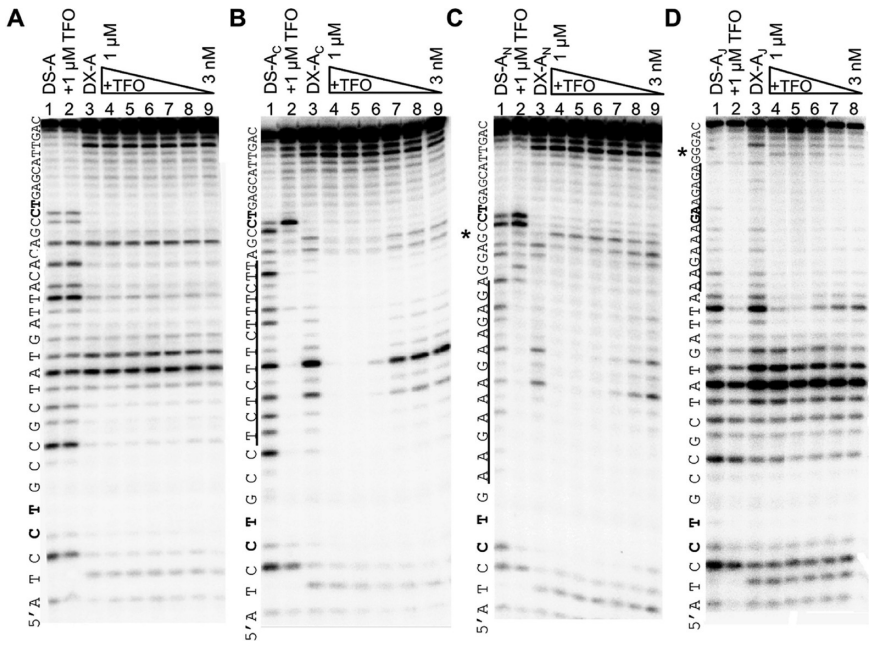

Figure 4. DNase I footprinting of DX tiles. DNase I cleavage patterns for the DX-A (A), DX-A_C (B), DX-A_N (C), and DX-A_J (D) tiles in the presence and absence of TFO. The non-crossover strand of the DX tile (sequence shown on the right of each gel) was labeled at its 5′-end with ^{32}P and annealed with the remaining strands at a final concentration of 0.1 μM. The TFO was then added to a final concentration of 0.1, 0.3, 1, 3, 10, and 30 μM (lanes 3−9) and left to equilibrate for >8 h at 4 °C before digestion with DNase I. Samples were run on a denaturing 14% PAGE gel, and the gel was fixed, dried, and subjected to phosphorimaging. An additional duplex control containing the labeled non-crossover strand and its complementary crossover strand (DS-A_X) was also digested in the presence and absence of TFO (lanes 1 and 2). Underlined regions denote the triplex target site, and the bold letters in the sequence on the right of each gel reflect the bases flanking each side of the two crossover points. The asterisk denotes regions of DNase I hypersensitivity.

the cleavage patterns reveal footprints for the TFOs only at their intended positions. As the proximity of the TFO to the junction seemed to have little influence on triplex formation, we also examined whether it was possible to target a TFO to a region that spanned the crossover itself, generating a three-way junction composed of four strands. A DX tile was designed to contain the same 13 bp oligopurine tract as above but this time on the non-crossover strand spanning the junction (Figure 2C; DX-A_J). The gel in Figure 4D shows the cleavage pattern from DNase I digestion of DX-A_J in the presence and absence of the 13-mer TFO. A clear footprint is evident that spans the full oligopurine target site, while the remaining cleavage pattern remained unaffected. DNase I hypersensitivity is also observed at the triplex−duplex junction at the 5′-end of the oligopurine target site (marked by an asterisk). Surprisingly, the presence of the crossover junction did not stop the TFO interacting with the non-crossover strand within the DX complex.

The pyrimidine triplex motif described here is not the only motif capable of generating triplex structures. Triplex formation with TFOs composed of purine bases is also possible by generating G.GC and A.AT triplets.[40] In this case, the TFO binds in an antiparallel orientation relative to the central strand of the target duplex. We therefore examined whether an appropriate purine-containing oligonucleotide was capable of targeting a DX tile in the same manner as before. However, these experiments revealed that the TFO was not capable of binding to the DX tile (Supplementary Figure 4). This is not surprising since it is well-established that this motif is intrinsically less stable that the pyrimidine binding motif.[40]

We also examined the underlying structure of the DX tiles in the presence or absence of TFO by circular dichroism (Supplementary Figure 5). There was no discernible difference between the spectra obtained for the DX tiles alone or in the presence of the TFO, suggesting no change to the underlying structure. In some instances, triplexes have been shown to exhibit an increased negative band at 220 nm compared to the equivalent duplex.[46] It has been suggested that this is due to changes in the sugar pucker (S-type > N-type) of both duplex and triplex strands upon formation of the complex. There are two possible reasons why this is not observed here. First, the contribution of signal from the region that has undergone triplex formation is much smaller than that of the remainder of the DX molecule and may therefore be masked. Alternatively, as the formation of a DX tile requires an integer of half-helical turns between crossovers, this may prevent any changes to the sugar pucker; conversion to an N-type configuration would make the helix more A-like, resulting in an increase in the helical repeat.

Targeting of a DX-A_CB Array. We next examined whether a TFO can access its binding site on a DX tile incorporated

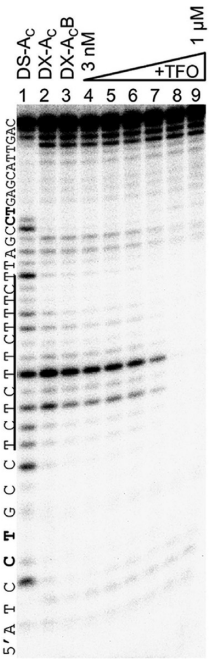

Figure 5. DNase I footprinting of a DX array. DNase I cleavage patterns for the DX-A$_C$ tile assembled with DX-B in the presence and absence of TFO. The non-crossover strand of the DX-A$_C$ tile (sequence shown on the right of the gel) was labeled at its 5′-end with ^{32}P and annealed with the remaining strands at a final concentration of 0.1 μM. This tile was mixed with an equimolar concentration of the DX-B tile and slowly annealed. The TFO was then added to a final concentration of 0.3, 1, 3, 10, and 30 μM (lanes 3−9) and left to equilibrate for >8 h at 4 °C before digestion with DNase I. Samples were run on a denaturing 14% PAGE gel, and the gel was fixed, dried, and subjected to phosphorimaging. Two additional controls were also run on the gel: a duplex containing the labeled non-crossover and complementary crossover strand (DS-A$_C$) and a DX-A$_C$ tile (lanes 1 and 2). Underlined regions denote the triplex target site, and the bold letters in the sequence on the right of each gel reflect the bases flanking each side of the two crossover points.

into a repeating DX-A$_C$B array. The DX-A$_C$B array was generated using the same DX-A$_C$ tile as examined above and a new DX tile (DX-B) containing complementary sticky ends at each of its four duplex termini (Figure 1A). The DX-B tile did not include a binding site for the TFO, and experiments revealed that the TFO was incapable of interacting with this tile, even at a 300-fold higher concentration (Supplementary Figure 6). Triplex formation at every other tile within the DX-A$_C$B array positions the TFO with a repeat spacing of 32 nm (94 nucleotides apart).

To examine the ability of the TFO to interact with the DX-A$_C$ tile in the context of a DX-A$_C$B array, the DX-A$_C$ tile was first annealed in the presence of a single ^{32}P-labeled strand, then mixed and annealed with the unlabeled DX-B tile. The final complex was then subjected to DNase I digestion in the presence and absence of various concentrations of TFO. The double-stranded (DS-A$_C$) and double-crossover (DX-A$_C$) complexes examined above were also digested and run on the same gel for comparison. The DNase I cleavage patterns for these structures are shown in

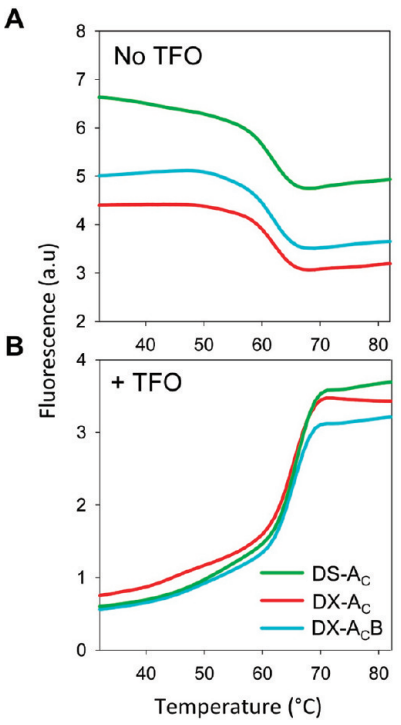

Figure 6. Fluorescence melting of the DX-A$_{C\#}$ tile and DX-A$_{C\#}$B array. The crossover strand of the DX-A$_{C\#}$ tile was labeled internally with FAM-C6-dT and assembled into the DS-A$_{C\#}$ duplex, DX-A$_{C\#}$ tile, and DX-A$_{C\#}$B array. The complexes were heated and cooled in a Roche LightCycler at a final concentration of 1 μM in the absence (A) or presence of the dabcyl-labeled TFO (B) at a final concentration of 10 μM. The samples were excited at 488 nm, and the subsequent fluorescence emission was recorded at 520 nm.

Figure 5. Comparing the digestion pattern in the absence of TFO (lanes 1−3) again reveals differences in the cutting pattern between the DS-A$_C$ and DX-A$_C$ complexes but no difference between DX-A$_C$ tile and the DX-A$_C$B array. This is not surprising since the structure of the DX-A$_C$ tile is unlikely to change in the presence of the DX-B tile. Further analysis of the digestion pattern in the presence of TFO (lanes 4−9) reveals a clear footprint at the same position to that observed for the isolated DX-A$_C$ complex above (Figure 4B). The footprints again disappear at lower concentrations of TFO. The data therefore suggest that the access of the TFO to DX-A$_C$ is not hindered by the adjacent DX-B tile in the context of the DX-A$_C$B array.

To examine the thermal stability of the triplex formed on both the DX tile and DX array and to compare these with the thermal stability of the underlying DX tiles, the complexes were appropriately labeled with fluorophores and examined in a Roche LightCycler.[47] An oligonucleotide with the same sequence as the crossover strand of DX-A$_C$ was synthesized with a fluorophore attached to a T at the 5′-end of the oligopurine target site (Figure 2C). This strand was then incorporated in a double-stranded (DS-A$_{C\#}$), double-crossover tile (DX-A$_{C\#}$), and array (DX-A$_{C\#}$B). After annealing, the complexes were heated at a sufficiently

slow rate and a decrease in fluorescence was observed as the complex dissociated (Figure 6A). A decrease in fluorescence occurs because FAM exhibits a higher fluorescence when associated with double-stranded DNA.[44] A single melting transition was observed for all complexes with an almost identical melting temperature of 60 °C. It is important to note that only the melting of the underlying helix is observed, not the melting of the full tile or array, which presumably occurs at a lower temperature.

The same experiments were repeated in the presence of a 13-mer TFO labeled at its 5′-end with the fluorescence quencher dabcyl. Upon triplex formation, the quencher is positioned in close proximity to the fluorophore within the DS-$A_{C\#}$, DX-$A_{C\#}$, and DX-$A_{C\#}$B complexes, and the fluorescence is quenched. Therefore, heating the samples resulted in an increase in fluorescence as the third strand dissociated. A single melting transition was again observed, with an identical melting temperature of 65 °C for all three complexes (Figure 6B). This confirms that the TFO can interact equally well with its duplex target irrespective of whether it is located in a DX tile or array. Surprisingly, it also suggests that the affinity of the TFO for its target on the DX tile is greater than that of the underlying duplex at the same region.

Further melting experiments were undertaken with different concentrations of the TFO and showed that the melting temperature of the triplex was concentration-dependent (Supplementary Figure 7A). The influence of pH on the binding of the TFO was also examined, and the melting temperature of the triplex decreased as the pH of the solution was increased (Supplementary Figure 7B). This is as expected since binding of the TFO is dependent on protonation of third strand cytosine bases.

Recruitment of Streptavidin to a DX Tile and Array. In the experiments described above, the assembly of the DX array in the presence and absence of TFO was not observed directly. We therefore examined whether the binding of the TFO to the DX-A_CB array could be visualized by AFM. A sample of the DX-A_CB array in the presence and absence of TFO was spotted onto freshly cleaved mica, dried, and imaged by tapping mode AFM in air. However, the resulting images revealed no difference between the complexes (data not shown). This is not surprising since binding of a TFO occurs within the duplex major groove and leads to only a slight increase in helical dimensions. We therefore chose to target the DX-A_CB array with an oligonucleotide conjugated to biotin and to recruit streptavidin to these positions to act as a visual marker. Before undertaking the AFM experiments, we first determined whether the addition of biotin influenced the binding of the TFO to an individual DX-A_C tile using the DNase I protection assay. These experiments revealed no difference in either the position or the affinity of TFO binding (Supplementary Figure 8). We also confirmed that streptavidin could be recruited to the TFO while attached to the tile by using an EMSA (data not shown).

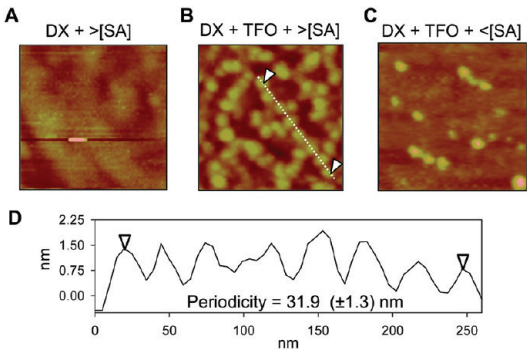

Figure 7. AFM of a DX-A_CB array. (A) Image of a sample containing the DX array and an excess of streptavidin (SA). (B) Image of a sample containing the DX array, the biotin-TFO, and an excess of SA. (C) Image of a sample containing the DX array, the biotin-TFO, and a lower concentration of SA. (D) Section analysis of the region representing the dotted white line in image shown in (B). All images are of a 300 × 300 nm section of the mica.

To ascertain whether the streptavidin molecules can interact with the DX-A_CB array in the absence of the biotin-TFO, a sample was prepared and imaged on mica (Figure 7A). The resulting image reveals clear patches on the mica surface that can be attributed to DNA lattices of various sizes. Section analysis of these patches reveals a height of 1.8 (±0.4) nm, which is in good accordance with a monolayer of DNA.[6] Moreover, no additional peaks are observed that suggest streptavidin is associated with either the DNA or the mica surface. We next examined whether the TFO was capable of recruiting streptavidin to the DX array. An image of a sample containing the DX-A_CB array, the biotin-TFO, and an excess of streptavidin is shown in Figure 7B. Unlike the previous image, several additional blobs are observed corresponding to a streptavidin molecule bound to the biotin-TFO associated with the array. In places, this is seen as a string of adjacent streptavidin molecules and can be attributed to regions where these molecules have been recruited to every other DX tile. Section analysis through one of these regions reveals an average spacing of 31.9 (±1.3) nm between streptavidin molecules (Figure 7D), in good agreement with the calculated distance between TFOs bound to every other DX tile. Further analysis of other adjacent streptavidin molecules reveals an overall average spacing of 31.5 ± 3.2 nm (Supplementary Figure 9). The recruitment of streptavidin was also dependent on the concentration of the added streptavidin; as expected, a concentration that was lower than that of the TFO resulted in fewer molecules being recruited (Figure 7C). Taken together, these results demonstrate successful targeting of a protein to specific locations within a DX array.

CONCLUSIONS

Here we have demonstrated that the triplex approach to DNA recognition can be successfully exploited to recognize specific loci within a DX tile and array. Before this study, we were concerned that access of an oligonucleotide to a duplex target site embedded between two crossover junctions might be difficult or impossible. The closely packed nature of the helices and the close proximity of the crossovers to the oligonucleotide target sequence might have occluded binding of the oligonucleotide. These concerns were clearly unfounded since target sites placed in different orientations and locations along the DX molecule were accessible to the binding of TFOs of various lengths and sequences. The dimensions of the interhelical gap in double- and multi-crossover molecules had previously been estimated to be between 1 and 2 nm depending on the distance between adjacent crossovers (1.5 to 2.5 helical turns).[9] These dimensions evidently allow an oligonucleotide to wrap around its target helix and generate a triple-stranded structure.

Interestingly, an oligopurine site positioned on the non-crossover strand of the helix, at a region that spanned the crossover junction, could also be targeted by a TFO. This is possible since binding of the oligonucleotide within the major groove is asymmetric, with the oligonucleotide recognizing only the purine-containing strand of the duplex. To our knowledge, this is the first example of a triple-helical crossover junction and gives rise to the possibility of designing structures based on this motif. In the past, the ability to generate two-dimensional arrays from single-crossover junctions has been hampered by their lack of rigidity and the tendency of the two helical domains to stack on one another. It would therefore be interesting to examine whether a triple-helical junction exhibits the same properties or whether it can act to make the junction more rigid and/or prevent helical stacking. It would also be interesting to examine whether the binding of an oligonucleotide could halt branch migration at crossovers generated between homologous duplexes.

The results presented here also demonstrate that, by conjugating biotin to the end of the oligonucleotide, streptavidin molecules can be recruited to precise locations within the DX array, with an average spacing of 31.9 (±1.3) nm. In this study, this was simply to aid in the visualization of the bound TFO, but this has significant implications for the ability to introduce components at precise locations within a DNA nanostructure. A variety of other chemical modifications compatible with oligonucleotide synthesis could be incorporated in a similar manner. These modifications could either be incorporated directly (*i.e.*, cross-linking agents, fluorophores, quenchers, *etc.*) or be used to bind or recruit other molecules, such as proteins and nanoparticles (*i.e.*, thiols, amines, alkyne carboxylic acids, *etc.*). Furthermore, the pH dependence of triplex formation could be exploited as a means to reverse the binding of the oligonucleotide at a later stage by adjusting the pH conditions. This would introduce read-write-erase functionality into a DNA nanostructure.

The approach described in this paper could be usefully applied to the wide variety of DNA nanostructures assembled by crossover strand exchange, such as those generated using double–double[7] and triple-crossover tiles,[8] as well as those that employ tiles in which the helices are not collinear.[10–14] In each case, this would require a simple modification to tile design so as to include an oligopurine target sequence necessary for triplex formation. However, in some cases, the choice of the embedded sequence may have to obey more stringent design rules that minimize sequence symmetry and promote the correct assembly of the structure. Most tile structures are designed so that a sequence of 6 consecutive base pairs occurs only once throughout the complex. Since an oligopurine target site only contains 2 different bases, this gives rise to 2^6 possible 6 bp combinations that could be incorporated. Furthermore, to generate the most stable triplexes, the oligopurine sequence should be asymmetric and avoid any repeating tracts, especially contiguous guanines, and the ratio of AT and GC base pairs kept roughly equal.

The design of some DNA nanostructures might not be amenable to the introduction of oligopurine target sequences, most notably, structures generated by DNA origami since these rely on the folding of the single-stranded M13mp18 DNA using short oligonucleotides and are therefore restricted to oligopurine sites already present within this sequence. At first sight, this might seem like a significant drawback of this approach, but simple analysis of the M13mp18 sequence reveals at least three oligopurine sites of >10 nucleotides that are compatible with triplex formation, the longest of which contains a run of 20 purines. There are also 10 oligopurine tracts that contain a single pyrimidine base within the tract and a further 3 that contain 2 pyrimidine bases. Since it has been shown that triplexes can be generated with one or two pyrimidines within the oligopurine sequence, these could also be targeted by appropriate TFO design. For example, guanine and thymine can be used to recognize TA and CG base pairs, generating G.TA and T.CG triplets, respectively.[40] Alternatively, the desired oligopurine–oligopyrimidine target site could be incorporated into the M13mp18 DNA scaffold by simple mutagenesis.

This sequence restriction is only a problem when using unmodified TFOs, and in recent years, a significant research effort has gone into extending triplex formation to mixed sequences by using TFOs containing nucleoside analogues. We and others have characterized a variety of these analogues and have shown

that it is possible to extend triplex formation to mixed sequence targets.[48−50] It is likely that these will be useful in the recognition of unique sequences within extended DNA nanostructures.

EXPERIMENTAL METHODS

Oligonucleotides and Synthesis. All oligonucleotides were synthesized on an Applied Biosystems ABI 394 automated DNA/RNA synthesizer on the 0.2 or 1 μM scale using standard methods. Phosphoramidite monomers and other reagents were purchased from Applied Biosystems or Link Technologies. The oligonucleotides for each DX tile were unmodified, except for DX-$A_{C\#}$, which contained an internal FAM-C6-dT (Glen Research). Triplex-forming oligonucleotides were either unmodified or contained a 5′-biotin or 5′-dabcyl (Link Technologies). The full sequences of the oligonucleotides used in this study are shown in Supplementary Table 1.

Annealing of Oligonucleotides. The oligonucleotides of each DX tile (or relevant control complex) were mixed stoichiometrically at an appropriate concentration (0.1−1 μM) in TA-Mg buffer (pH 5.0 40 mM Tris-acetate containing 15 mM magnesium acetate) and annealed at a rate of 0.5 °C min^{-1} in a thermocycler from 100 to 5 °C. For the formation of the DX array, equal amounts of the appropriate assembled DX tiles were mixed and annealed at a slower rate of 0.25 °C min^{-1} from 50 to 5 °C.

Electrophoretic Mobility Shift Assay. Each oligonucleotide was phosphorylated at its 5′-end with γ-^{32}P[ATP] using T4 polynucleotide kinase (New England Biolabs), purified by denaturing PAGE, and mixed with an excess of unlabeled oligonucleotide (1 μM). The unlabeled TFO (0.3−30 μM) was added either before or after the annealing of the DX tile and left to equilibrate for >8 h at 4 °C. The complexes were run on a nondenaturing 8% PAGE gel in TA-Mg buffer at 4 °C, and the gel was fixed, dried, and subjected to phosphorimaging.

DNase I Protection Assay. The non-crossover oligonucleotide of each DX tile (or relevant control complex) was phosphorylated at its 5′-end with γ-^{32}P[ATP] using T4 polynucleotide kinase (New England Biolabs) and purified by denaturing PAGE. It was then combined with the remaining oligonucleotides (0.1 μM) and annealed as before. The TFO (0.03−1 μM) was added either before or after the annealing of the DX tile and left to equilibrate for >8 h at 4 °C. The resulting complexes were mixed with 2 μL of DNase I (typically 0.01 units/mL) dissolved in 20 mM NaCl containing 2 mM $MgCl_2$ and 2 mM $MnCl_2$. The reaction was stopped after 1 min by adding 4 μL of DNase I stop solution [80% formamide, 10 mM EDTA, 10 mM NaOH, and 0.1% (w/v) bromophenol blue]. The products of digestion were separated on a denaturing 14% PAGE gel, and the gel was fixed, dried, and subjected to phosphorimaging. Samples were heated to 100 °C for 3 min before loading onto the gel.

Fluorescence Melting. Fluorescence melting with the complexes was carried out using a Roche LightCycler as previously described.[44] In these experiments, the TFO was labeled at its 5′-end with a quencher (dabcyl), while the purine-containing strand of the DX tile (or relevant control) was labeled at an internal position with FAM-C6-dT. The complexes were first denatured by rapidly heating to 95 °C and left to equilibrate for 10 min. The complexes were then cooled to 30 °C at a rate of 0.2 °C min^{-1} to eliminate hysteresis. After 5 min, the complexes were heated to 95 °C at the same temperature gradient. Although the slowest rate of continuous temperature change in the LightCycler is 0.1 °C s^{-1}, slower melting profiles were obtained by increasing the temperature in 1 °C steps, leaving the samples to equilibrate for a set amount of time. Recordings were taken during both the heating and cooling steps to check for hysteresis. T_m values were determined from the first derivatives of the melting profiles using the software provided with the machine and usually differed by less than 0.5 °C.

Atomic Force Microscopy. Samples were prepared with various combinations of DX-A_CB array (0.1 μM), TFO (1 μM), and streptavidin (0.2 or 2 μM). These were then spotted onto freshly cleaved mica and allowed to adsorb for 5 min. Buffer salts were removed by addition of 5−10 drops of ultrapure water from an Elga UHQ-II water purification system with a resistivity of 18 MΩ·cm; the drop was shaken off and the sample dried using compressed air. Imaging was undertaken by tapping mode in air on a Multimode AFM equipped with a Nanoscope III controller using silicon nitride cantilever tips (Nanoworld Pointprobes, k = 2.8 N/m).

Conflict of Interest: The authors declare no competing financial interest.

Acknowledgment. This work was supported from BBSRC grant BB/H019219/1.

Supporting Information Available: Additional experimental details and results (Table S1, Figures S1−9). This material is available free of charge *via* the Internet at http://pubs.acs.org.

REFERENCES AND NOTES

1. Seeman, N. C. Nanomaterials Based on DNA. *Annu. Rev. Biochem.* **2010**, *79*, 65–87.
2. Pinheiro, A. V.; Han, D.; Shih, W. M.; Yan, H. Challenges and Opportunities for Structural DNA Nanotechnology. *Nat. Nanotechnol.* **2011**, *6*, 763–772.
3. Torring, T.; Voight, N. V.; Nangreave, J.; Yan, H.; Gothelf, K. V. DNA Origami: A Quantum Leap for Self Assembly of Complex Structures. *Chem. Soc. Rev.* **2011**, *40*, 5636–5646.
4. Bath, J.; Turberfield, A. J. DNA Nanomachines. *Nat. Nanotechnol.* **2007**, *2*, 275–284.
5. Fu, T.; Seeman, N. C. DNA Double-Crossover Molecules. *Biochemistry* **1993**, *32*, 3211–3220.
6. Winfree, E.; Liu, F.; Wenzler, L. A.; Seeman, N. C. Design and Self-Assembly of Two-Dimensional DNA Crystals. *Nature* **1998**, *394*, 539–544.
7. Reishus, D.; Shaw, B.; Brun, Y.; Chelyapov, N.; Adleman, L. Self-Assembly of DNA Double−Double Crossover Complexes into High-Density, Doubly Connected, Planar Structures. *J. Am. Chem. Soc.* **2005**, *50*, 17590–17591.
8. LaBean, T. H.; Yan, H.; Kopatsch, J.; Liu, F.; Winfree, E.; Reif, J. H.; Seeman, N. C. Construction, Analysis, Ligation, and Self Assembly of DNA Triple Crossover Complexes. *J. Am. Chem. Soc.* **2000**, *122*, 1848–1860.
9. Rothemund, P. W. K. Folding DNA To Create Nanoscale Shapes and Patterns. *Nature* **2005**, *440*, 297–302.
10. Malo, J.; Mitchell, J. C.; Turberfield, A. J. A Two-Dimensional DNA Array: The Three-Layer Logpile. *J. Am. Chem. Soc.* **2009**, *131*, 13574–13575.
11. Liu, D.; Wang, M.; Deng, Z.; Walulu, R.; Mao, C. Tensegrity: Construction of Rigid DNA Triangles with Flexible Four-Arm DNA Junctions. *J. Am. Chem. Soc.* **2004**, *126*, 2324–2325.
12. Constantinou, P. E.; Wang, T.; Kopatsch, J.; Israel, L. B.; Zhang, X.; Ding, B.; Sherman, W. B.; Wang, X.; Zheng, J.; Sha, R.; *et al.* Double Cohesion in Structural DNA Nanotechnology. *Org. Biomol. Chem.* **2006**, *4*, 3414–3419.
13. He, Y.; Chen, Y.; Liu, H.; Ribbe, A. E.; Mao, C. Self-Assembly of Hexagonal DNA Two-Dimensional (2D) Arrays. *J. Am. Chem. Soc.* **2005**, *127*, 12202–12203.
14. Yan, H.; Park, S. H.; Finkelstein, G.; Reif, J. H.; LaBean, T. H. DNA-Templated Assembly of Protein Arrays and Highly Conductive Nanowires. *Science* **2003**, *301*, 1882–1884.
15. Douglas, S. M.; Chou, J. J.; Shih, W. M. DNA-Nanotube-Induced Alignment of Membrane Proteins for NMR Structure Determination. *Proc. Natl. Acad. Sci. U.S.A.* **2007**, *104*, 6644–6649.
16. Zheng, J.; Birktoft, J. J.; Chen, Y.; Wang, T.; Sha, R.; Constantinou, P. E.; Ginell, S. L.; Mao, C.; Seeman, N. From

Molecular to Macroscopic *via* the Rational Design of a Self-Assembled 3D DNA Crystal. *Nature* **2009**, *461*, 74–77.
17. Wang, T.; Sha, R.; Birktoft, J.; Zheng, J.; Mao, C.; Seeman, N. C. A DNA Crystal Designed To Contain Two Molecules per Asymmetric Unit. *J. Am. Chem. Soc.* **2010**, *132*, 15471–15473.
18. Malo, J.; Mitchell, J.; Venien-Bryan, C.; Harris, R.; Wille, H.; Sherratt, D. J.; Turberfield, A. J. Engineering a 2D Protein-DNA Crystal. *Angew. Chem.* **2005**, *44*, 3057–30621.
19. Selmi, D. N.; Adamson, R. J.; Attrill, H.; Goddard, A. D.; Gilber, R. J. C.; Watts, A.; Turberfield, A. J. DNA-Templated Protein Arrays for Single Molecule Imaging. *Nano Lett.* **2011**, *11*, 657–660.
20. Kuzuya, A.; Sakai, Y.; Yamazaki, T.; Xu, Y.; Komiyama, M. Nanomechanical DNA Origami 'Single-Molecule Beacons' Directly Imaged by Atomic Force Microscopy. *Nat. Commun.* **2011**, *2*, 1–8.
21. Lin, C.; Katilius, E.; Liu, Y.; Zhang, J.; Yan, H. Self-Assembled Signalling Aptamer DNA Arrays for Protein Detection. *Angew. Chem., Int. Ed.* **2006**, *45*, 5296–5301.
22. Robinson, B.; Seeman, N. C. The Design of a Biochip: A Self-Assembling Molecular-Scale Memory Device. *Protein Eng.* **1987**, *1*, 295–300.
23. Mao, C.; LaBean, T. H.; Relf, J. H.; Seeman, N. C. Logical Computation Using Algorithmic Self Assembly of DNA Triple-Crossover Molecules. *Nature* **2000**, *407*, 493–496.
24. Rothemund, P. W. K.; Papadakis, N.; Winfree, E. Algorithmic Self-Assembly of DNA Sierpinski Triangles. *PLoS Biol.* **2004**, 2041–2053.
25. Barish, R. D.; Schulman, R.; Rothemund, P. W.; Winfree, E. An Information-Bearing Seed for Nucleating Algorithmic Self-Assembly. *Proc. Natl. Acad. Sci. U.S.A.* **2009**, *106*, 6054–6059.
26. Wilner, O. I.; Weizmann, Y.; Gill, R.; Lioubashevski, O.; Freeman, R.; Willner, I. Enzyme Cascades Activated on Topologically Programmed DNA Scaffolds. *Nat. Nanotechnol.* **2009**, *4*, 249–254.
27. Voigt, N. V.; Tørring, T.; Rotaru, A.; Jacobsen, M. F.; Ravnsbaek, J. B.; Subramani, R.; Mamdouh, W.; Kjems, J.; Mokhir, A.; Besenbacher, F.; *et al.* Single-Molecule Chemical Reactions on DNA Origami. *Nat. Nanotechnol.* **2010**, *5*, 200–203.
28. Li, H.; Park, S. H.; Reif, J. H.; LaBean, T. H.; Yan, H. DNA-Templated Self Assembly of Protein and Nanoparticle Linear Arrays. *J. Am. Chem. Soc.* **2004**, *126*, 418–419.
29. Lund, K.; Liu, Y.; Lindsay, S.; Yan, H. Self-Assembling a Molecular Pegboard. *J. Am. Chem. Soc.* **2005**, *127*, 17606–17607.
30. Williams, B. A. R.; Lund, K.; Liu, Y.; Yan, H.; Chaput, J. C. Self-Assembled Peptide Nanoarrays: An Approach To Studying Protein−Protein Interactions. *Angew. Chem., Int. Ed.* **2007**, *46*, 3051–3054.
31. Kuzyk, A.; Laitinen, K. T.; Torma, P. DNA Origami as a Nanoscale Template for Protein Assembly. *Nanotechnology* **2009**, *20*, 1–5.
32. Shen, W.; Zhon, H.; Neff, D.; Norton, M. L. NTA Directed Protein Nanopatterning on DNA Origami Nanoconstructs. *J. Am. Chem. Soc.* **2009**, *131*, 6660–6661.
33. Rinker, S.; Ke, Y.; Liu, Y.; Chhabra, R.; Yan, H. Self-Assembled DNA Nanostructures for Distance-Dependent Multivalent Ligand-Protein Binding. *Nat. Nanotechnol.* **2008**, *3*, 418–422.
34. Liu, Y.; Lin, C.; Li, H.; Yan, H. Aptamer-Directed Self-Assembly of Protein Arrays on a DNA Nanostructure. *Angew. Chem., Int. Ed.* **2005**, *44*, 4333–4338.
35. Li, H.; LaBean, T. H.; Kenan, D. J. Single-Chain Antibodies Against DNA Aptamers for Use as Adapter Molecules on DNA Tile Arrays in Nanoscale Materials Organization. *Org. Biomol. Chem.* **2006**, *4*, 3420–3426.
36. Xiao, S.; Liu, F.; Rosen, A. E.; Hainfield, J. F.; Seeman, N. C.; Musier-Forsyth, K.; Kiehl, R. A. Self-Assembly of Metallic Nanoparticles Arrays by DNA Scaffolding. *J. Nanopart. Res.* **2002**, *4*, 313–317.
37. Le, J. D.; Pinto, Y.; Seeman, N. C.; Musier-Forsyth, K.; Taton, A. T.; Kiehl, R. A. DNA-Templated Self-Assembly of Metallic Nanocomponent Arrays on a Surface. *Nano Lett.* **2004**, *4*, 2343–2347.
38. Dutta, P. K.; Varghese, R.; Nangreave, J.; Lin, S.; Yan, H; Liu, Y. DNA-Directed Artificial Light-Harvesting Antenna. *J. Am. Chem. Soc.* **2011**, *133*, 11985–11993.
39. Cohen, J. D.; Sadowski, J. P.; Dervan, P. Addressing Single Molecules on DNA Nanostructures. *Angew. Chem., Int. Ed.* **2007**, *46*, 7956–7959.
40. Moser, H. E.; Dervan, P. B. Sequence Specific Cleavage of Double-Helical DNA by Triple Helix Formation. *Science* **1987**, *238*, 645–648.
41. Le Doan, T.; Perrouault, L.; Praseuth, D.; Habhoub, N.; Decout, J. L.; Thuong, N. T.; Lhomme, J.; Hélène, C. Sequence-Specific Recognition, Photocrosslinking and Cleavage of the DNA Double Helix by an Oligo-[α]-thymidylate Covalently Linked to an Azidoproflavine Derivative. *Nucleic Acids Res.* **1987**, *19*, 7749–7760.
42. Hélène, C.; Toulmé, J. J. Specific Regulation of Gene Expression by Antisense, Sense and Antigene Nucleic Acids. *Biochim. Biophys. Acta* **1990**, *1049*, 99–125.
43. Fox, K. R. Targeting DNA with Triplexes. *Curr. Med. Chem.* **2000**, *7*, 17–37.
44. Tumpane, J.; Kumar, R.; Lundberg, E. P.; Sandin, P.; Gale, N.; Nandhakumar, I. S.; Albinsson, B.; Wilhelmsson, L. M.; Brown, T.; Norden, B. Triplex Addressability as a Basis for Functional DNA Nanostructures. *Nano Lett.* **2007**, *7*, 3832–3839.
45. Cardew, A. S.; Brown, T.; Fox, K. R. Secondary Binding Sites for Heavily Modified Triplex Forming Oligonucleotides. *Nucleic Acids Res.* **2012**, 10.1093/nar/gkr1119.
46. Gray, D. M.; Hung, S.; Johnson, K. H. Absorption and Circular Dichroism Spectroscopy of Nucleic Acids Duplexes and Triplexes. *Methods Enzymol.* **1995**, *245*, 19–34.
47. Darby, R. A.; Sollogoub, M.; McKeen, C.; Brown, L.; Risitano, A.; Brown, N.; Barton, C.; Brown, T.; Fox, K. R. High Throughput Measurement of Duplex, Triplex and Quadruplex Melting Curves Using Molecular Beacons and a LightCycler. *Nucleic Acids Res.* **2002**, *30*, e39.
48. Rusling, D. A.; Powers, V. E.; Ranasinghe, R. T.; Wang, Y.; Osborne, S. D.; Brown, T.; Fox, K. R. Four Base Recognition by Triplex-Forming Oligonucleotides at Physiological pH. *Nucleic Acids Res.* **2005**, *33*, 3025–3032.
49. Buchini, S.; Leumann, C. J. Stable and Selective Recognition of Three Base Pairs in the Parallel Triple-Helical DNA Binding Motif. *Angew. Chem., Int. Ed.* **2004**, *43*, 3925–3928.
50. Li, S.; Chen, F. X.; Shikiya, R.; Marky, L. A.; Gold, B. Molecular Recognition *via* Triplex Formation of Mixed Purine/Pyrimidine DNA Sequences Using OligoTRIPs. *J. Am. Chem. Soc.* **2005**, *127*, 12657–65.